"ACTIVE FLUX" SENSORLESS VECTOR CONTROL OF IPMSM FOR WIDE SPEED RANGE

Mihaela Codruta PAICU[*], Lucian TUTELEA[*], *Member, IEEE*,
Gheorghe Daniel ANDREESCU[**], *Senior Member, IEEE*, Ion BOLDEA[*], *Fellow, IEEE*
[*]Dept. of Electrical Engineering, [**]Dept. of Automation and Applied Informatics,
University Politehnica of Timisoara, 2 Vasile Parvan Blvd., 300223 Timisoara, Romania

Abstract. *This paper presents a novel torque control strategy for the sensorless control of IPMSM. The proposed torque control strategy includes a new reference torque calculation method that is capable to develop maximum toque possible of the motor for an optimal current pair (i_d, i_q) below rated speed, but also in flux weakening region (above rated speed) where voltage and current limitations impose constraints on the allowable (i_d, i_q) currents. The motion sensorless control of the IPMSM is obtained via model-based stator flux estimation using the "active flux" concept. A comprehensive digital simulation of a wide speed motion sensorless control of IPMSM drive, operating down to 1 rpm and up to 6000 rpm demonstrates the effectiveness of the proposed control system. Experiments are due soon.*

Keywords: *sensorless vector control, low speed operation, high speed operation, maximum torque per ampere, flux-weakening.*

1. Introduction

Interior PM synchronous motors are becoming more and more favored in wide speed range applications. Eliminating the shaft position sensor is welcome, based on cost and reliability constraints.

Thus, in the last few years the search for position sensorless control has emerged, involving very low [1]-[7] and also very high speed. In the last case, it is difficult to make the acquisition of speed signal from the incremental encoder.

Below rated speed, the maximum torque per ampere strategy (MTPA) is used to produce torque with the smallest possible stator current amplitude and to keep this way the copper loss at minimum [8]-[15].

Above rated speed, the torque capability of a synchronous motor is limited by the maximum current and the maximum voltage that the inverter can apply to the motor.

Flux weakening operation is mandatory to produce the maximum torque that the machine could possibly develop at high speeds [16]-[22].

In this paper, for the motion sensorless control, the "active flux" observer was used, from which accurate rotor position and speed estimation are obtained.

The "active flux" concept (or "torque producing flux"), which "turns all the salient–pole machines into nonsalient–pole ones" was developed in [5].

Though this concept is useful especially in achieving low speed operation, here it is used for wide speed operation.

We include a torque close loop with a new reference torque calculation method that takes magnetic saturation into account. This method consists in providing maximum toque capability of the motor for an optimal current pair (i_d, i_q) below rated speed, but also in flux weakening region (above rated speed) where voltage and current limitations impose constraints on the allowable (i_d, i_q) currents.

To extend the torque/speed range automatic rearrangement of (i_d^*, i_q^*) is provided.

In conclusion, the optimal d and q axis currents fully utilize the inverter capability, while maximizing the output torque and power.

This proposed vector control strategy ensures that the machine is operated reasonably, close to optimal efficiency, for all loads.

The digital simulation results demonstrate proper motion-sensorless operation down to 1 rpm and up to 6000 rpm, without any signal injection.

2. Mathematical model of ipmsm

The mathematical model of a saturated IPMSM in the d-q synchronous reference frame is given by:

$$\overline{V}_s = R_s \cdot \overline{i}_s + \frac{d\overline{\psi}_s}{dt} + j\omega_r \cdot \overline{\psi}_s \qquad (1)$$

$$\overline{\psi}_s = L_d(i_d) \cdot i_d + (L_q \cdot i_q - \psi_{PMq}) \qquad (2)$$

$$T_e = \frac{3}{2} \cdot p_1 \cdot \left[\psi_{PMq} + (L_d(i_d) - L_q) \cdot i_q\right] \cdot i_d \qquad (3)$$

where V_s is the stator voltage, i_s is the stator current, R_s is the stator resistance, L_d, L_q are the d-q axes inductances, ψ_s is the stator flux, ψ_{PMq} is the PM flux linkage, T_e is the electromagnetic torque, ω_r is the electrical rotor speed and p_1 is the number of pole pairs.

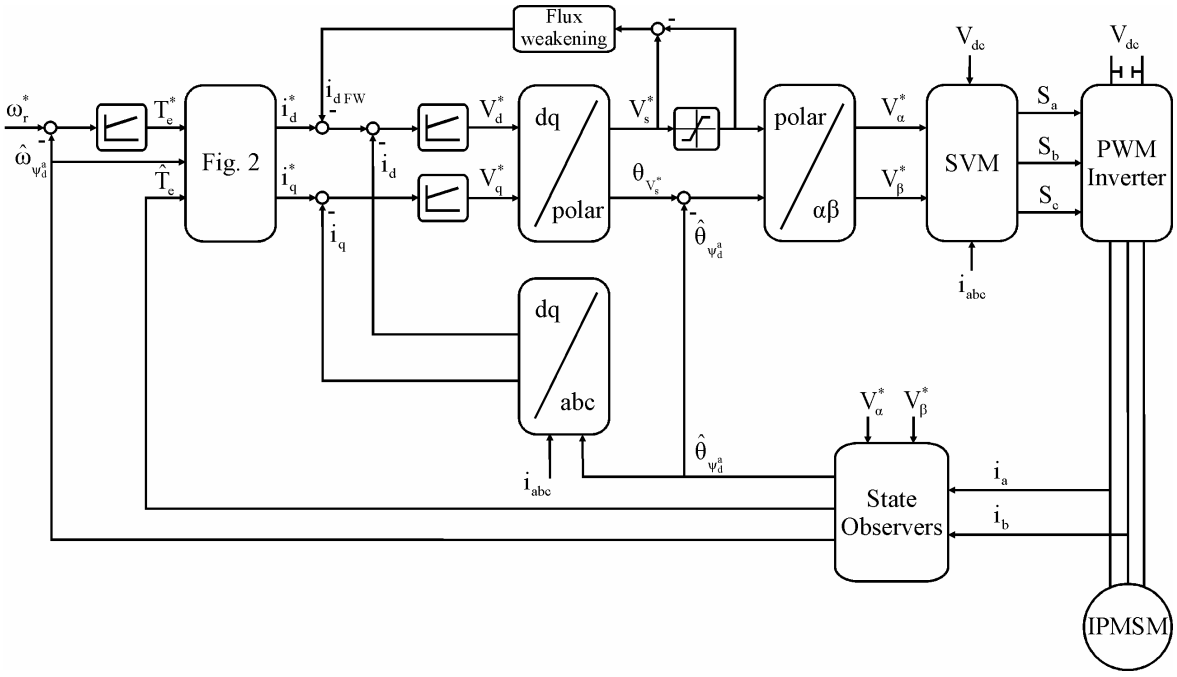

Fig. 1. The proposed sensorless control system

3. Sensorless control system

Fig. 1 illustrates the proposed sensorless control system for IPMSM, which consists in torque control strategy scheme, space vector modulator block (SVM), active flux observer and rotor position-speed estimator.

As in usual vector control, the two PI current control loops have been implemented in a synchronous rotating *dq* reference frame having a better performance than stationary frame regulators, as they operate on dc quantities.

The d component of the stator current acts on the stator flux, whereas the q component acts on the torque.

The design of the controllers employs the relation (4):

$$k_p(1+\frac{k_i}{s}) \tag{4}$$

The proportional and integral gains for the PI controller were chosen by trial and are given in Table 2 (see APPENDIX).

The SVM block generates the switching signals for the voltage source inverter.

The state observers provide rotor position, rotor speed and torque estimators, in order to achieve sensorless control of the IPMSM drive.

Let us now present the torque control strategy.

A speed controller provides the reference torque.

For a certain speed the torque can be achieved with a variety of different d–q current pairs. For each d–q current pair a particular torque value is obtained.

There is an optimum operating point ($i^*_{d\_opt}, i^*_{q\_opt}$) in which for a demanded torque, the line current amplitude is minimized.

The upper part of the Fig. 2 illustrates that the d axis current component i^*_d is obtained by minimizing two curves: the magnetizing curve ($i^*_d(\psi^*_{sd})$) and $i^*_{d\_opt}(T^*_e)$ curve, which is obtained by Finite Element Method (FEM).

The lower part of the Fig. 2**,** illustrates how the q axis current component i^*_q is obtained.

Based on the torque error between the reference and the estimated one, the PI torque controller produces a torque request by adjusting the q current component $i^*_{q\_opt}$ according to (3) for given T^*_e and $i^*_{d\_opt}$.

The output signal of the PI torque controller is forwarded by a speed dependent torque curve.

The signal obtained is then limited by the maximum q current component value for a certain speed ($i^*_{q\_\max}(\omega^*_r)$).

Using the torque control strategy described so far, the reference current components i^*_d and i^*_q always ensure that the magnitude of the stator current vector does not exceed the maximum current $I_{s\max}$:

$$\sqrt{i_d^2+i_q^2} \le I_{s\max} \tag{5}$$

In conclusion, below rated speed the current limit (5) and the rated flux level ψ^*_s determine the operating point corresponding to the maximum torque.

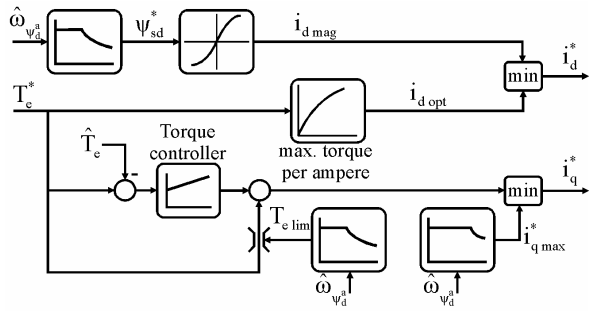

Fig. 2. The current references

Above base speed, the torque control strategy is based on the flux weakening control method because here we need to reduce the stator flux magnitude in order to satisfy the voltage constraint:

$$\sqrt{V_d^2 + V_q^2} \le V_{s\max} \tag{6}$$

$V_{s\max}$ is the maximum voltage capability of the inverter.

The voltage limitation (flux weakening) block from the Fig. 1 ensures though $i_{d\,FW}^*$ that the voltage reference satisfies the voltage constraint.

The angular phase of the reference voltage in *dq* coordinates, $\theta_{V_s^*}$ is added to the estimated angle rotor position in order to ensure the machine operation in the stator reference frame.

While operating in the base speed range, the condition (6) holds. In this case, the reference stator flux ψ_s^* is limited to its rated value.

If the voltage provided from the regulators exceeds its maximum value $V_{s\max}$, the excitation of the machine is then reduced by reducing the reference stator flux value ψ_s^*.

In order to accomplish this, a substantial reduction of the magnetizing current i_d^* (till 60% from it), though $i_{d\,FW}^*$, must be done.

The current margin that is thus gained allows increasing the torque producing current component i_q^*.

In conclusion, the operating point of the maximum possible torque corresponding to a certain speed value is defined by the intersection of the two curves: the voltage limit curve and the current limit curve.

To obtain fast torque dynamics when operating at the voltage limit, in [21]-[22], for an induction machine case, a temporary voltage margin is created in a dynamic condition by deviating the trajectory of the stator flux linkage vector to flux values of lower magnitude.

To accomplish this, the scheme illustrated in Fig. 3 is used. As it can be seen the speed error $\Delta\omega$ is used as a feedforward signal. A reaction is enabled by the condition $\Delta V_s \le 0$ that indicates operation at or close to the maximum available voltage. A signal $\Delta\delta$ (varying between 0 and 60 degrees) is then created and it rotates the stator voltage vector such that the stator flux linkage vector is deviated towards a trajectory of reduced diameter.

In our IPMSM case, the temporary voltage margin is already created by the torque control strategy itself, and thus the scheme presented in Fig. 1 does not need to be used here. To demonstrate this, digital simulations operating at the voltage limit without and with $\Delta\delta$ are presented in Fig. 5.

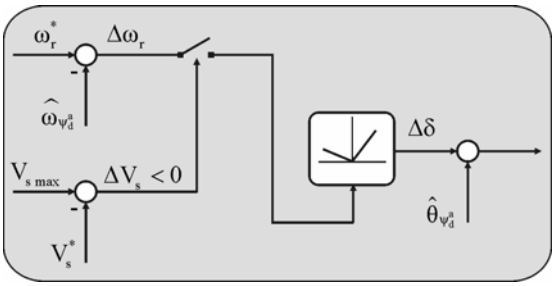

Fig. 3. The variation angle scheme

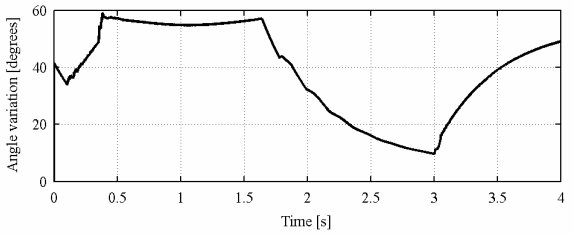

Fig. 4. Torque transients from 1 Nm to 3 Nm during operation at the maximum available voltage (6000 rpm): angle variation correction $\Delta\delta$

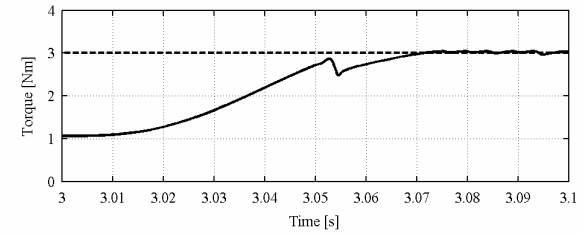

Fig. 5. Torque transients from 1 Nm to 3 Nm during operation at the maximum available voltage (6000 rpm): reference (dashed line) and actual torque when operating without the angle variation correction $\Delta\delta$

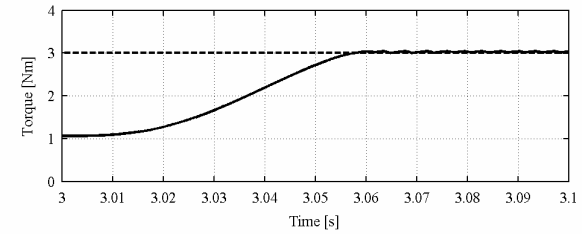

Fig. 6. Torque transients from 1 Nm to 3 Nm during operation at the maximum available voltage (6000 rpm): reference (dashed line) and actual torque when operating with the angle variation correction $\Delta\delta$

As it can be seen the results are similar, though with $\Delta\delta$ contribution the torque response is smoother and a bit faster, at maximum speed of 6000 rpm.

4. State observers

4.1 Active Flux Observer

This observer is based on the "active flux" concept, as developed in [5].

The main claim of the "active flux" concept is that it turns all salient-pole rotor ac machines into fictitious nonsalient-pole ones such that the rotor position and speed estimation become simpler.

This means that it leads to the estimation of both "active flux" amplitude ψ_d^a and angle $\theta_{\psi_d{}^a}$ with respect

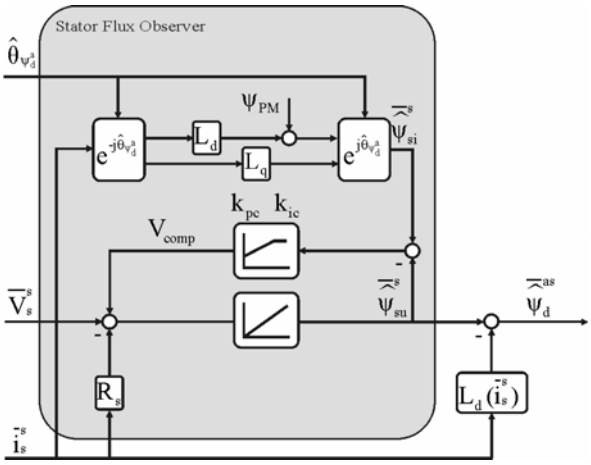

Fig. 7. The stator flux observer

to stator phase *a* (for our IPMSM case $\theta_{\psi_d{}^a} = \theta_{er} + \frac{\pi}{2}$ (where θ_{er} is the electrical angle rotor position)).

For our IPMSM case, the "active flux" vector $\bar{\psi}_d^a$ observer, in stator coordinates, is:

$$\bar{\psi}_d^{as} = \int (\bar{V}^s_s - R_s \bar{i}^s_s + V_{comp})dt - L_d \bar{i}^s_s \qquad (7)$$

$$\bar{\psi}_d^{as} = \bar{\psi}^s_s - L_d(i_s) \cdot \bar{i}^s_s \qquad (8)$$

where V_{comp} is the voltage compensation based on the current flux model and it employs the following equation, as it can be observed in Fig. 7:

$$V_{comp} = (k_p + \frac{k_i}{s})(\bar{\psi}^s_{si} - \bar{\psi}^s_{su}) \qquad (9)$$

The proportional and integral gains for the PI compensator were chosen by trial and are given in Table 2 (see APPENDIX).

In practical use, V_{comp} is compensating the various errors in the $\bar{\psi}_d^{as}$ estimation as inverter nonlinearities (power switch voltage drop, dead-time), integration dc-offset, stator resistance correction, magnetic saturation.

The operating principle for this observer is to extract the "active flux" information from the measured stator currents and reference stator voltages.

The active flux observer implementation scheme is presented in Fig. 7 and it consists in a stator flux observer in stator coordinates from which the term $L_d(i_s) \cdot \bar{i}^s_s$ is subtracted(7).

The stator flux observer combines advantages of the current model) at low speed with the voltage model at medium-high speed, using a compensation loop driven by the stator flux estimation error.

4.2 Position-Speed Estimator

The overall performance of the motion sensorless control depends strongly on the accuracy of the rotor position and speed estimation.

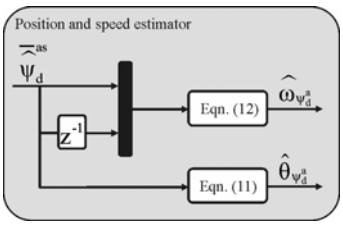

Fig. 8. The position-speed observer

The rotor position-speed estimator implementation is illustrated in Fig. 8.

Usually a PLL (phase-locked-loop) estimator is used for rotor position-speed estimation. In what follows, however, we make use of the estimator in (10)- Fig. 9 below:

$$\omega_{\psi_d^a} = \frac{d\hat{\theta}_{\psi_d^a}}{dt} \qquad (10)$$

$$\hat{\theta}_{\psi_d^a} = \text{atan}(\frac{\psi^a_{d\beta}}{\psi^a_{d\alpha}}) \qquad (11)$$

$$\omega_{\psi_d^a} = \frac{\psi^a_{d\alpha k-1}\psi^a_{d\beta} - \psi^a_{d\beta k-1}\psi^a_{d\alpha}}{h(\psi^{a\ 2}_{d\alpha} + \psi^{a\ 2}_{d\beta})} \qquad (12)$$

where *h* is the sampling time, and the index *k*-1 in Fig. 10denotes variables delayed with one sampling period.

The position estimator estimates the active flux rotor position $\hat{\theta}_{\psi_d{}^a}$ and the electrical speed $\omega_{\psi_d^a}$.

The estimated angle $\hat{\theta}_{\psi_d{}^a}$ is used for supplying all vector transformations between the *abc* and *dq* frames.

The rotor speed estimation $\omega_{\psi_d^a}$ in the whole speed range is required in the speed controller.

4.3 Torque Estimato

The estimated torque is obtained from (3), using the estimated stator flux components and the measured current components in stationary reference frame.

5. Digital simulations results

The digital simulation using the proposed sensorless vector control strategy has been processed in MATLAB/Simulink package for the IPMSM model specified in Table 1 (see APPENDIX).

The following digital simulation tests are performed to check the proposed sensorless vector control strategy:

a. Start up response from 0 to the lowest speed of 1 rpm followed by a full step torque load (Fig. 11 - Fig. 19)
b. Start up response from 0 to the maximum speed of 6000 rpm followed by a step load at 37% rated (base) torque (Fig. 20 - Fig. 30).

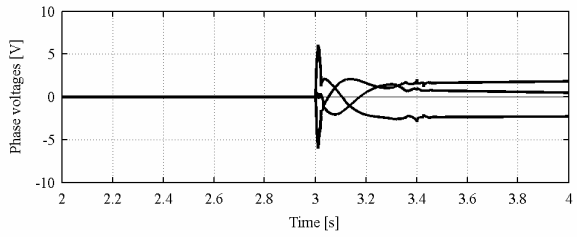

Fig. 11. Start up response from 0 to 1 rpm followed by a full step torque load: stator phase voltages (V_a, V_b, V_c)

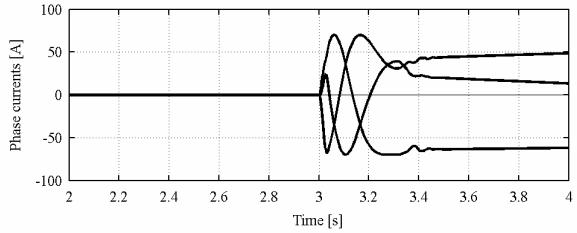

Fig. 12. Start up response from 0 to 1 rpm followed by a full step torque load: stator phase currents (i_a, i_b, i_c)

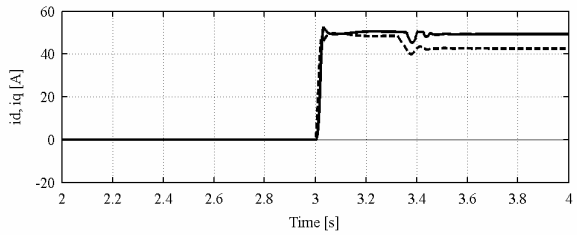

Fig. 13. Start up response from 0 to 1 rpm followed by a full step torque load: the d-q axes currents i_d (dashed line) and the q axis current i_q

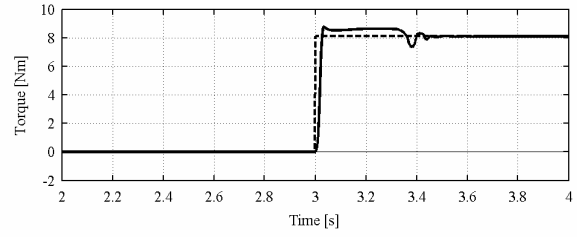

Fig. 14. Start up response from 0 to 1 rpm followed by a full step torque load: reference (dashed line) and actual torque

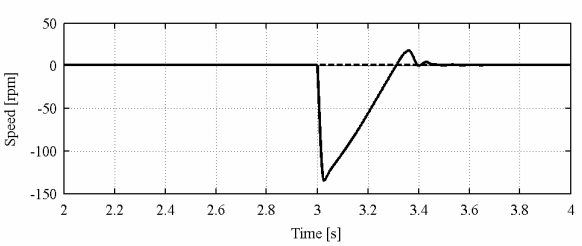

Fig. 15. Start up response from 0 to 1 rpm followed by a full step torque load: reference (dashed line) and actual speed

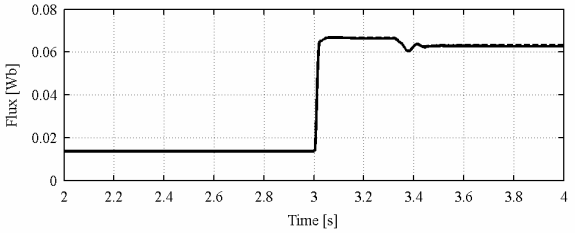

Fig. 16. Start up response from 0 to 1 rpm followed by a full step torque load: the actual (dashed line) and estimated flux

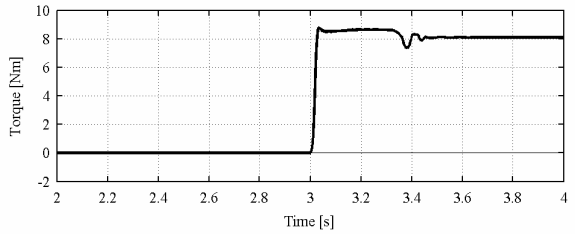

Fig. 17. Start up response from 0 to 1 rpm followed by a full step torque load: actual (dashed line) and estimated torque

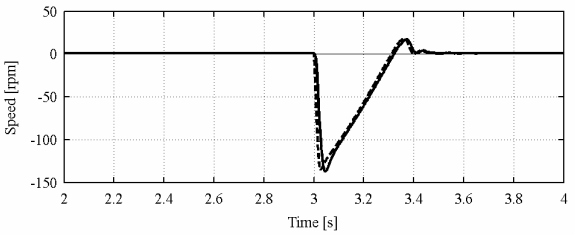

Fig. 18. Start up response from 0 to 1 rpm followed by a full step torque load: actual (dashed line) and estimated speed

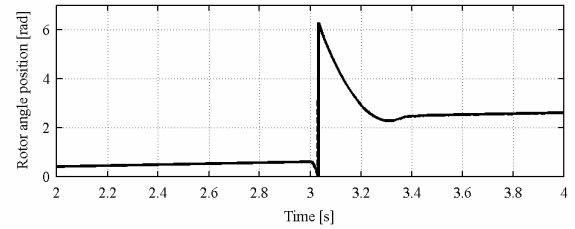

Fig. 19. Start up response from 0 to 1 rpm followed by a full step torque load: actual and estimated rotor angle position

The actual speed is also given for reference.

The Fig. 15 shows a quick speed recovery.

Fig. 16shows that the flux increases at flux reference value only during torque transients in order to produce the

demanded torque; otherwise it is maintained at the PM flux (low) value.

The same speed ripple in the actual speed waveform is visible in the estimated speed waveform (Fig. 18).

The position estimation during torque transients is very reliable (Fig. 19).

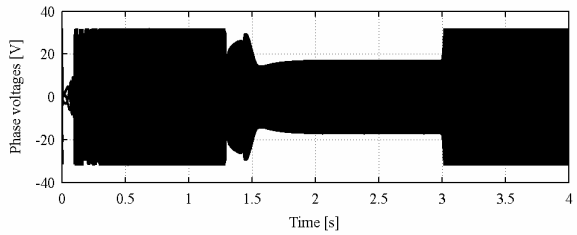

Fig. 20. Start up response from 0 to 6000 rpm followed by a step load at 37% rated torque: stator phase voltages (V_a, V_b, V_c)

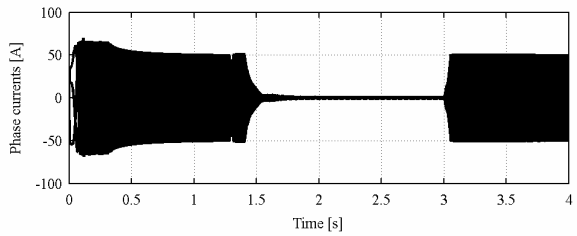

Fig. 21. Start up response from 0 to 6000 rpm followed by a step load at 37% rated torque: stator phase currents (i_a, i_b, i_c)

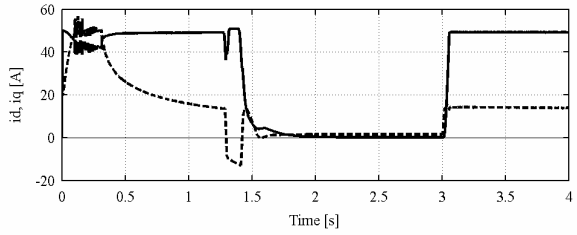

Fig. 22. Start up response from 0 to 6000 rpm followed by a step load at 37% rated torque: the d-q axes currents i_d (dashed line) and the q axis current i_q

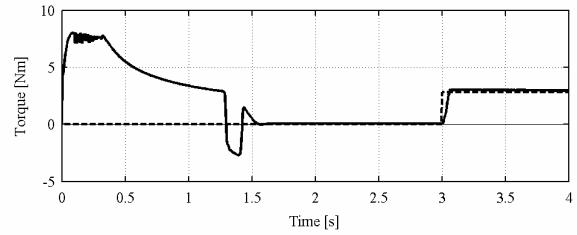

Fig. 23. Start up response from 0 to 6000 rpm followed by a step load at 37% rated torque: reference (dashed line) and actual torque

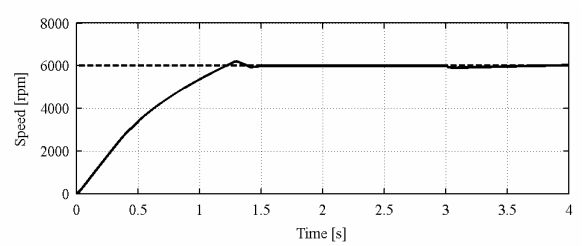

Fig. 24. Start up response from 0 to 6000 rpm followed by a step load at 37% rated torque: reference (dashed line) and actual speed

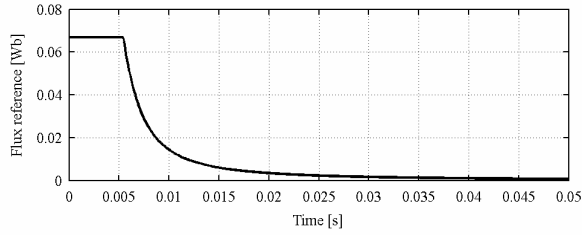

Fig. 25. Start up response from 0 to 6000 rpm followed by a step load at 37% rated torque: the flux reference curve

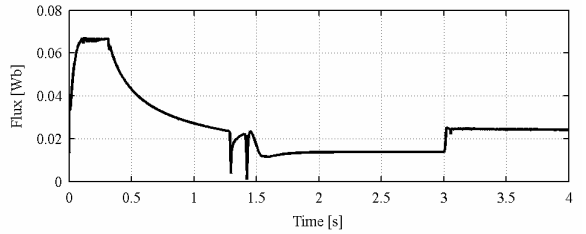

Fig. 26. Start up response from 0 to 6000 rpm followed by a step load at 37% rated torque: the actual and estimated flux

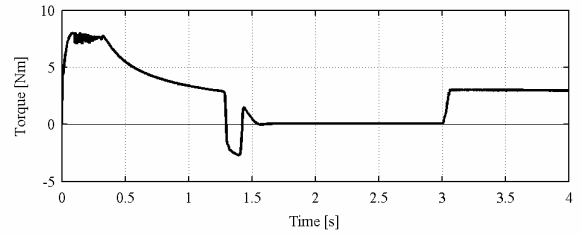

Fig. 27. Start up response from 0 to 6000 rpm followed by a step load at 37% rated torque: actual and estimated torque

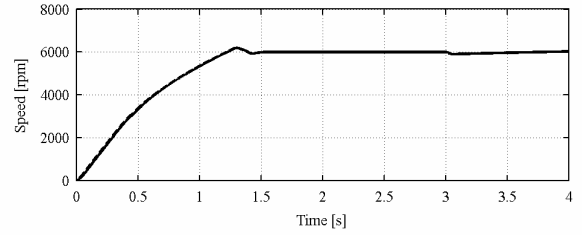

Fig. 28. Start up response from 0 to 6000 rpm followed by a step load at 37% rated torque: actual (dashed line) and estimated speed

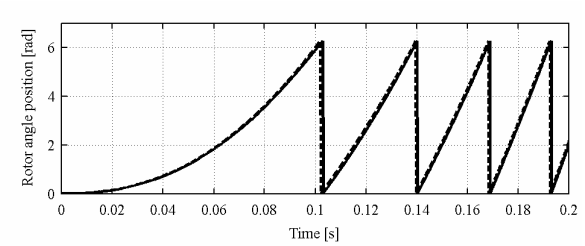

Fig. 29. Start up response from 0 to 6000 rpm followed by a step load at 37% rated torque: zoom of actual (dashed line) and estimated rotor angle position at start up

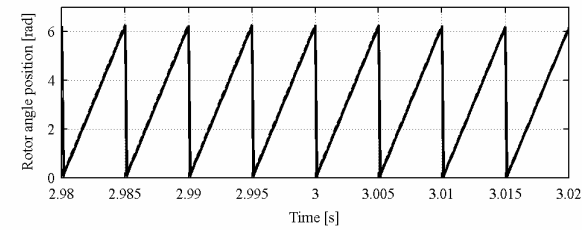

Fig. 30. Start up response from 0 to 6000 rpm followed by a step load at 37% rated torque: zoom of actual (dashed line) and estimated rotor angle position at step load torque

Fig. 20-Fig. 30 illustrate start up to 6000 rpm transients with step load perturbation.

The voltage and current reduction after start up shows clearly the optimum torque/flux relationship to reduce losses at high speed and low torque.

From Fig. 20 and Fig. 21 it is clear that during torque transients at 6000 rpm the machine uses the entire available voltage and current.

Fig. 25 illustrates the flux reference curve in the flux weakening operation mode.

Fig. 26 shows how, once the actual speed achieves the reference speed value, the flux is decreased until it achieves the PM flux linkage (low) value.

Fig. 28 shows that above rated speed, when the flux weakening operation is reached (see also the torque curve in Fig. 27), the speed increases smoother than during the operation below rated speed.

The estimated rotor position follows very well the actual rotor position even when the speed reference or load disturbance change quickly, as it is shown in Fig. 29 and Fig. 30.

As the magnetization curve $\psi_d(i_d)$ is considered, only at medium speeds the stator resistance error influences to some extent the active flux angle (rotor angle) position estimation.

6. Conclusion

The claim of the proposed torque control strategy is a new reference torque calculation and close loop method that is capable to develop maximum torque possible of the motor for an optimal current pair (i_d , i_q) below rated speed, but also in flux weakening region (above rated speed) where voltage and current limitations impose constraints on the allowable (i_d , i_q) currents.

At low speed the voltage constraint does not effect the operation of the motor. But at higher speed (FW region) the voltage constraint becomes more effective. To avoid reaching the voltage constraint, the d-axis current should be controlled in such a way that it will weaken the magnetic flux.

Using the proposed control strategy the motor uses the maximum torque capability in the whole speed range, maintaining the voltage and current constraints.

The rotor position and speed estimation from the "active flux" is used in order to achieve robust sensorless control of the IPMSM.

The effectiveness of the proposed model-based sensorless control strategy is confirmed by digital simulation, which operates down to 1 rpm and up to 6000 rpm.

7. Appendix

Table 1.

Parameters of the prototype IPMSM

Number of pole pairs (p)	2
Rated power	2.2 kW
Rated speed	2500 rpm
Rated frequency	83.33 Hz
Rated torque	8.2 Nm
Rated phase to phase voltage	22 V(rms)
Rated phase current	50 A(rms)
Stator resistance per phase (Rs)	0.037 Ω
d-axis inductance (Ld)	1.62 mH
q-axis inductance (Lq)	0.45 mH
Rotor permanent - magnet (λPM)	0.0136 V s rad-1
Inertia of the rotating system (J)	1x10-3 kgm2
Viscous friction coefficient (Bm)	1x10-4Nms/rad

TABLE 2.

GAINS USED IN DIGITAL SIMULATION

PI speed controller	k_{p_w}	1
	k_{i_w}	20
PI torque controller	k_{p_T}	1
	k_{i_T}	1000
PI i_d controller	$k_{p\_i_d}$	10
	$k_{i\_i_d}$	400
PI i_q controller	$k_{p\_i_q}$	10
	$k_{i\_i_q}$	100

References

[1] E. Urlep and K. Jezernik, "Low and zero speed sensorless control of nonsalient PMSM," in *Conf. Record IEEE-ISIE 2007*, pp. 2238–2243.

[2] C. Silva, G. M. Asher, and M. Sumner, "Hybrid rotor position observer for wide speed range sensorless PM motor drives including zero speed," *IEEE Trans. Ind. Electron.*, vol. 53, no. 2, pp. 373–378, 2006.

[3] A. Consoli, G. Scarcella, and A. Testa, "Industry applications of zero speed sensorless control techniques for PMSMs," *IEEE Trans. Ind. Appl.*, vol. 37, no. 2, pp. 513–521, 2001.

[4] G. D. Andreescu, C. I. Pitic, F. Blaabjerg, and I. Boldea, "Combined flux observer with signal injection enhancement for wide speed range sensorless DTFC of IPMSM drives,"*IEEE Trans. Energy Convers.*, vol. 23, no. 2, pp. 393–402, 2008.

[5] I. Boldea, M. C. Paicu, and G. D. Andreescu, "Active flux concept for motion sensorless unified ac drives," *IEEE Trans. Power Electron.*, (to be published).

[6] I. Boldea, M. C. Paicu, and G. D. Andreescu, "Active flux orientation vector sensorless control of IPMSM," in *Proc. OPTIM 2008*, vol. 2, pp. 161-168.

[7] I. Boldea, M. C. Paicu, G. D. Andreescu and F. Blaabjerg, "Active flux DTFC-SVM sensorless control of IPMSM," *IEEE Trans. Energy Convers.*, (to be published).

[8] G. Kang, J. Lim, K. Nam, H.B. Ihm and H.G.. Kim, "A MTPA control scheme for an IPM synchronous motor considering magnetic flux variation caused by temperature," in *Proc. IEEE-APEC 2004*, vol. 2, pp. 1617-1621.

[9] C.T. Pan and S.M. Sue, "A linear maximum torque per ampere control for IPMSM drives over full-load range speed," *IEEE Trans. Energy. Convers.*, vol. 20, no. 2, pp. 359–366, 2005.

[10] E.M. Rashad, T.S. Radwan, and M. A. Rahman, "A maximum torque per ampere vector control strategy for synchronous reluctance motors considering saturation and iron losses," in *Proc. IEEE-IEMDC-2003*, vol. 2, pp. 1211–1217.

[11] Z.C. Zhu, Y. S. Chen and D. Howe, "Iron loss in permanent-magnet brushless ac machines under maximum torque per ampere and flux weakening control," *IEEE Trans. Magn.*, vol. 38, no. 5, pp. 3285–3287, 2002.

[12] C.B. Butt, M.A. Hoque and M.A. Rahman, "Simplified fuzzy-logic-based MTPA speed control of IPMSM drive," *IEEE Trans. Ind. Appl.*, vol. 40, no. 6, pp. 1529–1535, 2004.

[13] Y. A. R. I. Mohamed and T.K. Lee, "Adaptive self-tuning MTPA vector controller for IPMSM: drive system," *IEEE Trans. Energy. Convers.*, vol. 21, no. 3, pp. 636–644, 2006.

[14] P. Niazi and H. Toliyat, "Robust maximum torque per ampere (MTPA) control," in *Conf. Record APEC 2006*.

[15] C. Butt and M.A. Rahman, "Limitations of simplified fuzzy logic in *Conf. Record IAC 2004*, vol. 3, pp. 1405–1410.

[16] M.I. Chy and M.N. Uddin, "A novel fuzzy logic controller based torque and controls of IPM synchronous motor," in *Conf. Record IAC 2007*, pp. 1844–1851.

[17] M.N. Uddin and M.I. Chy, "Development and implementation of a nonlinear controller incorporating flux control for IPMSM," in *Proc. IEEE-IECON-2007.*, vol. 40, no. 2, pp. 1067–1072, 2007.

[18] S. Morimoto, M. Sanada, and Y. Takeda, "Effects and compensation of magnetic saturation in flux-weakening controlled permanent magnet synchronous motor drives," *IEEE Trans. Ind. Appl.*, vol. 30, no. 6, pp. 1632–1637, 1994.

[19] M. N. Uddin and M. A. Rahman, "High speed control of IPMSM drives using improved fuzzy logic algorithms," *IEEE Trans. Ind. Electron.*, vol. 54, no. 1, pp. 190–199, 2007.

[20] J. Wai, and T.M. Jahns, "A new control technique for achieving wide constant power speed operation with an interior PM alternator machine," in *Conf. Record IEEE-IAS 2001*, vol. 2, pp. 807-814.

[21] M. Mengoni, L. Zarri, A. Tani, G. Serra, and D. Casadei, "Stator flux vector control of induction motor drive in the field weakening region," *IEEE Trans. Power Electron.*, vol. 23, no. 2, pp. 941–949, 2008.

[22] H. Abu-Rub, H. Schmirgel and J. Holtz, "Sensorless control of induction motors for maximum steady-state torque and fast dynamics at field weakening," in *Conf. Record IEEE-IAS 2006*, vol. 1, pp. 96–103.